Structural Characterization of Adenine Nucleotides Bound to *Escherichia coli* Adenylate Kinase. 1. Adenosine Conformations by Proton Two-Dimensional Transferred Nuclear Overhauser Effect Spectroscopy†

Yan Lin‡ and B. D. Nageswara Rao*

Department of Physics, Indiana University Purdue University Indianapolis (IUPUI), 402 North Blackford Street, Indianapolis, Indiana 46202-3273

Received August 17, 1999; Revised Manuscript Received December 3, 1999

ABSTRACT: Adenosine conformations of adenosine 5′-triphosphate (ATP) and adenosine 5′-monophosphate (AMP), and of an ATP analogue, adenylyl imidodiphosphate (AMPPNP), bound to *Escherichia coli* adenylate kinase (AKe) in the complexes of AKe·Mg(II)ATP, AKe·AMP·Mg(II)GDP, AKe·AMPPNP, and AKe·Mg(II)AMPPNP were determined by transferred two-dimensional nuclear Overhauser effect spectroscopy (TRNOESY) measurements and molecular dynamics simulations. The glycosidic torsion angles, χ, deduced for the adenine nucleotides in these complexes are 51°, 37°, 49°, and 47°, respectively, with an experimental error of about ±5°. These values are in general agreement with those previously measured for other ATP-utilizing enzymes, suggesting a possible common motif for adenosine recognition and binding. The pseudorotational phase angle, *P*, of the sugar puckers for the bound nucleotides varied between 50° and 103°. These solution-state conformations are significantly different from those in published data from X-ray crystallography. A computation of the ligand NOEs, made by using the program CORCEMA [Moseley, H. N. B., Curto, E. V., and Krishna, N. R. (1995) *J. Magn. Reson. B108*, 243−261] with the protein protons in the vicinity of nucleotide included, on the basis of the X-ray structure of the AKe·AMP·AMPPNP complex [Berry, M. B., Meador, B., Bilderback, T., Liang, P., Glaser, M., and Philips, G. N., Jr. (1994) *Proteins: Struct., Funct., Genet. 19*, 183−198], showed that polarization transfer to the protein protons does not produce significant errors in the structures determined by considering the ligand NOEs alone.

Adenylate kinase (AK),[1] the smallest known monomeric phosphoryl transferase with a molecular mass of 22−26 kDa, first isolated from rabbit muscle more than 50 years ago by Colowick and Kalckar (*1*), catalyzes reversible phosphoryl transfer from MgATP and ADP given by (*2*)

$$\text{AMP} + \text{MgATP} \Leftrightarrow \text{ADP} + \text{MgADP} \qquad (1)$$

The enzyme is ubiquitous in organisms, as it has the function of bringing AMP into the energy pool. AKs from many sources have been investigated by both X-ray crystallography and NMR. For example, for *Escherichia coli* AK (AKe), X-ray structures of three complexes, viz., apo-AKe (*3*), AKe·AP_5A (*4*), and AKe·AMP·AMPPNP (*5*), have been published so far. Historically, NMR studies on AK have shown agreements and disagreements with the results from X-ray crystallography with respect to the nucleotide binding sites. An in-depth review of these observations and results from X-ray, NMR, and mutagenesis studies on AK was given by Tsai and Yan (*6*). The currently accepted AMP and ATP binding sites are those suggested by the latest X-ray data (*7*−*9*) and supported by NMR (*10*, *11*) and site-directed mutagenesis (*12*).

However, information on the conformation of enzyme-bound substrates is scant, since no crystals of ATP or MgATP bound to any adenylate kinase have been obtained, thus far. Information regarding the ATP binding domain, and evidence for substrate-binding-induced movements of this domain, have been inferred on the basis of crystal structure differences between the apoenzyme and those with one or both nucleotide sites occupied by AMP, ATP analogue ($AMPPCF_2P$), and the bisubstrate inhibitor AP_5A (*9*, *13*). The functional groups involved in the substrate binding have not been identified. Furthermore, with the exception of yeast adenylate kinase (*14*), crystal structures fail to locate the cation at the active site. In addition to these inadequacies in the crystallographic data on the substrate conformation, there is considerable evidence for conformational differences

† Supported in part by National Institutes of Health (GM43966) and IUPUI. This work forms part of a thesis for which Y.L. was awarded a Ph.D. degree in physics by Purdue University in 1999. Part of these results were presented at the 39th Experimental NMR Conference (ENC) held at Asilomar, CA, March 22−27, 1998.

* To whom correspondence should be addressed: E-mail brao@iupui.edu.

‡ Present address: Department of Biochemistry & Biophysics, School of Medicine, University of Pennsylvania, Philadelphia, PA 19104-6059.

[1] Abbreviations: 2D, two-dimensional; ADP, adenosine 5′-diphosphate; AK, adenylate kinase; AKe, *Escherichia coli* adenylate kinase; AMP, adenosine 5′-monophosphate; AMPPNP, adenylyl-imidodiphosphate; AP_5A, P^1,P^5-bis(5′-adenosyl)pentaphosphate; ATP, adenosine 5′-triphosphate; DSS, 2,2-dimethyl-2-silapentanesulfonate; GDP, guanosine 5′-diphosphate; Hepes, *N*-(2-hydroxyethyl)piperazine-*N*′-2-ethanesulfonic acid; MD, molecular dynamics; NMR, nuclear magnetic resonance; NOE, nuclear Overhauser effect; PDB, protein data bank; RMSD, root-mean-squared deviation; Tris-d_{11}, deuterated tris(hydroxymethyl)aminomethane; TRNOESY, transferred two-dimensional nuclear Overhauser effect spectroscopy.

10.1021/bi991921t CCC: $19.00
Published on Web 03/07/2000

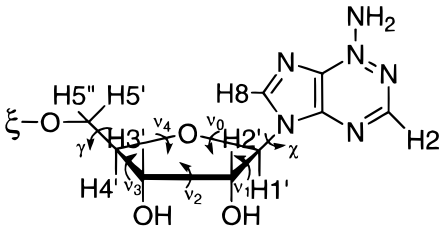

FIGURE 1: Chemical structure of adenosine moiety showing the numbering for the relevant protons and the torsion angles.

between bound substrate molecules in solution and crystalline states. For example, recent determinations of the glycosidic orientation of adenine nucleotide complexes of a number of ATP-utilizing enzymes in solution, characterized by torsion angle, χ (see Figure 1), made by the TRNOESY method (*15*−*19*), showed values of χ clustered in a narrow range of $52° \pm 8°$ (*18*). The ATP-utilizing enzymes studied belong to three categories: (a) phosphoryl-transfer enzymes, creatine kinase (*15*), arginine kinase (*16*), and pyruvate kinase (*17*); (b) an adenylyl-transfer enzyme, methionyl-tRNA synthetase (*18*); and (c) a pyrophosphoryl-transfer enzyme, PRibPP synthetase (*19*). Among these data, the value of 46° determined for χ in the recently published X-ray crystal structure of the transition-state analogue complex of arginine kinase (*20*) agrees well with the value of $50° \pm 5°$ obtained by NMR (*16*). In contrast, in the X-ray structures of just the AK complexes, the glycosidic torsion angles span from −9° for AMP in AKe·AMP·AMPPNP (*5*) to 107° for the ATP moiety of AP_5A in AKe·AP_5A (*4*). Panels A and B of Figure 2 show histograms of the glycosidic torsion angle, χ, obtained for various enzyme-bound adenine nucleotides from NMR and X-ray studies, respectively. The data used for Figure 2B were based on the X-ray structures available in the Brookhaven Protein Data Bank (PDB). The kinases included in the histogram all have a small molecule for the second substrate. Protein kinases are not included (see Supporting Information).

It is our goal to characterize the conformation of AMP and MgATP bound at the active site of AKe in the liquid phase with the help of high-resolution NMR measurements. The strategy used for the structure determination is based on the following reasoning. A nucleotide free in solution has three internal mobilities: the glycosidic rotation, the sugar pucker, and the overall flexibility of the phosphate chain. If the enzyme-bound nucleotide assumes a unique conformation, the characterization of such a conformation requires a specification of how these internal mobilities are frozen. There is evidence that the glycosidic reorientation of ATP is arrested upon binding to various ATP-utilizing enzymes (*21*). The glycosidic orientation and sugar pucker are determined by means of 2D proton TRNOESY experiments described in this paper. The orientation of the phosphate chain with respect to the adenosine moiety is determined on the basis of enhancement of nuclear relaxation rates of ^{31}P and ^{13}C nuclei (using [u-^{13}C]nucleotides) in the presence of substituent paramagnetic cations Co(II) and Mn(II), respectively. Results of these measurements will be presented in the accompanying paper (*22*).

The TRNOESY results presented in this paper include those on AKe complexes of AMPPNP, in addition to those on the AMP and MgATP complexes, in order to make a comparison with X-ray crystallographic data obtained with

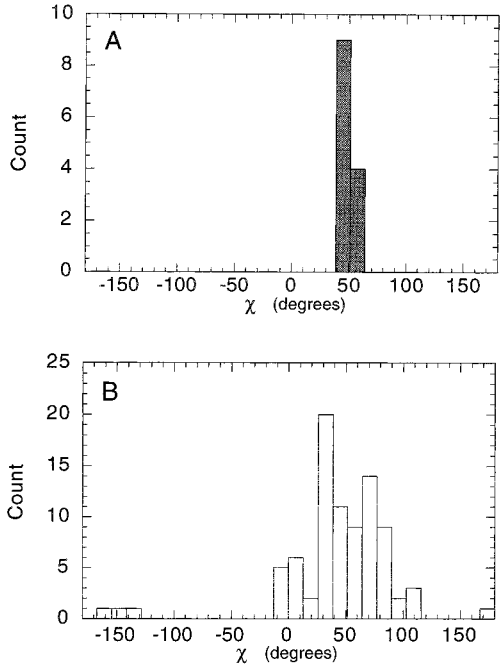

FIGURE 2: Histogram of glycosidic torsion angles measured for adenine nucleotides in enzyme-bound complexes. Resolution of the histogram is 10°. (A) Values obtained from NMR studies on ATP-utilizing enzymes; (B) Values measured from X-ray structures of nucleotide complexes of various ATP-utilizing enzymes (data collected from references given in the Supporting Information provided).

the ATP analogue. Since there are two nucleotide binding sites on the enzyme, the experiments were performed by choosing sample conditions to minimize possible binding of the nucleotides at the other site. Furthermore, the concentrations of the enzyme and substrates are optimized to minimize weak nonspecific binding of the nucleotides, which plagued some of the early TRNOE measurements on ATP-utilizing enzymes.

Uncertainties due to the effect of magnetization transfer to protein protons has been an unresolved issue in previously published TRNOE-determined adenosine conformations (*15*−*19*). A realistic evaluation of this effect could not be made in those cases due to the fact that the information regarding the location of protein protons with respect to these on the nucleotide was not available. Since crystallographic data are available for AKe complexes, a computation and evaluation of the effect of protein protons on the TRNOESY data and their analyses could be undertaken in the presented work. Results of this computation are included in this paper.

EXPERIMENTAL PROCEDURES

Materials. AMP, ATP, and AMPPNP were purchased from Sigma Chemical Co., DSS from Norell Chemical Co., GDP from Boehringer Manheim, DEAE-cellulose from Whatman, Blue Sepharose resin from Pharmacia, Hepes from Research Organics, and Chelex-100 from Bio-Rad. Deuterated tris(hydroxymethyl)aminomethane (Tris-d_{11}) and 99.9% D_2O were from Cambridge Isotope Labs. All other chemicals used were of analytical reagent grade.

Sample Preparation. An expression system of AKe was kindly provided by Professor Paul Rösch, Universität of Bayreuth, Bayreuth, Germany. The purification of the enzyme was performed following published procedures (*23*). The purity of the enzyme was ascertained by electrophoresis,

and the specific activity of the enzyme was assayed by monitoring the formation of ADP by coupling with pyruvate kinase and lactate dehydrogenase reactions (*2*). The specific activity of the enzyme is usually ~800 units/mg. In making NMR samples for TRNOESY experiments, the enzyme was concentrated to ~100 mg/mL by using Amicon ultrafiltration concentrators with YM series membranes of molecular weight cutoff no more than 5000. The buffer for the concentrated enzyme was exchanged to a D_2O solution of 50 mM Tris-d_{11}, pH 8.0, either by dialysis in a Spectrum block dialysis unit or by ultrafiltration with a 3 mL Amicon concentrator with YM-1 membrane. Nucleotides were prepared by dissolving in D_2O, adjusting pH to 8.0, and passing through a Chelex-100 column for removal of possible metal ion contamination. The solutions were then lyophilized and stored at −20 °C. The final dissolution of the nucleotides in D_2O was made immediately before addition to the enzyme. The concentrations of the nucleotides and of the enzyme were determined spectrophotometrically with extinction coefficients $\epsilon_{259}^{mM} = 15.4\ cm^{-1}$ for AMP, ATP, and AMPPNP, $\epsilon_{252}^{mM} = 13.7\ cm^{-1}$ for GDP, and $\epsilon_{280}^{mg/mL} = 0.5\ cm^{-1}$ for the enzyme (molecular mass 23.6 kDa) (*24*). The pH values reported are direct pH meter readings for the prepared samples, uncorrected for the presence of D_2O. All buffer solutions were passed through a Chelex-100 column to remove trace metal impurities.

NMR Measurements. The TRNOESY experiments were performed on a Varian UNITY-Plus 720 NMR spectrometer at the National High Magnetic Field Laboratory, Tallahassee, FL, and on a Varian INOVA 500 NMR spectrometer at the NMR Center of IUPUI. All the measurements were carried out at 15 °C. A typical sample composition used was 2.5 mM adenine nucleotide, 0.5 mM AKe, buffered in 50 mM Tris-d_{11}, pH 8.0, in a volume of ~700 μL. This protocol was chosen to minimize nonspecific-binding contribution while optimizing the transfer of NOE from bound complex to the free (see Results and Analysis section). For experiments with Mg(II)-chelated nucleotides, viz., Mg(II)ATP, Mg(II)AMPPNP, and Mg(II)GDP, Mg(II) was added to a final concentration at least twice that of the nucleotide in order to ensure complete saturation.

NOESY data were acquired in hypercomplex mode (*25*) with 2K (F_2) × 256 (F_1) data size for mixing times from 40 to 240 ms. For each t_1 increment, 32 scans and a relaxation delay of 2 s were used. Zero-quantum interference was suppressed by random variation of the mixing time up to 10% of its value between different t_1 increments (*26*). The carrier frequency was placed on the HDO resonance in all the experiments. The solvent resonance was suppressed by monochromatic irradiation using the decoupler channel during intervals of the relaxation delay, the t_1 period, and the mixing period. Data points were extended by a 4-fold forward linear prediction in the F_1 dimension, followed by Fourier transformation in both dimensions with a Gaussian apodization of 0.064 s, and zero-filling to a data set of 2K in F_1 and 4K in F_2. The spectra were phased to pure absorption mode. The diagonal peak intensity of H8 extrapolated to zero mixing time was used for NOE normalization.

Theoretical Details. The basic theory of TRNOESY can be found in many publications (*27*−*32*). It has been shown that under fast-exchange conditions, i.e., $\tau_b^{-1}, \tau_f^{-1} \gg (\mathbf{W}_b)_{ij}, (\mathbf{W}_f)_{ij}$, for times greater than $(\tau_b^{-1} + \tau_f^{-1})^{-1}$, the time evolution of the longitudinal magnetizations of an n-spin system is given by (*32*)

$$\frac{d}{dt}(\mathbf{m}_b + \mathbf{m}_f) \approx -\mathbf{R}(\mathbf{m}_b + \mathbf{m}_f) \approx -(p_b\mathbf{W}_b + p_f\mathbf{W}_f)(\mathbf{m}_b + \mathbf{m}_f) \quad (2)$$

where the subscripts b and f refer to bound state and free state, respectively, p_b and p_f are population fractions of the ligand, $\mathbf{m}_b$ and $\mathbf{m}_f$ are n-dimensional vectors with each element representing the deviation of the z-magnetization of a spin from its equilibrium value, $\mathbf{W}_b$ and $\mathbf{W}_f$ are $n \times n$ relaxation matrixes, and τ_b and τ_f are the lifetimes of the bound and free states, respectively. For homonuclear spin systems, if dipolar interaction is the only relaxation mechanism, the relaxation matrix elements of $\mathbf{W}_b$ and $\mathbf{W}_f$ are given by standard expressions (*32*−*35*):

$$\mathbf{W}_{ii} = \frac{\gamma^4\hbar^2\tau_c}{10}\left[1 + \frac{3}{1+\omega^2\tau_c^2} + \frac{6}{1+4\omega^2\tau_c^2}\right]\sum_{k\neq i} r_{ik}^{-6} \quad (3)$$

$$\mathbf{W}_{ij} = \mathbf{W}_{ji} = \frac{\gamma^4\hbar^2\tau_c}{10 r_{ij}^{6}}\left[-1 + \frac{6}{1+4\omega^2\tau_c^2}\right] \quad (4)$$

where γ and ω are the gyromagnetic ratio and Larmor frequency of the protons, r_{ij} is the distance between spin i and spin j, and τ_c is the isotropic rotational correlation time. r_{ij} and τ_c will correspond to free and bound species depending on whether $\mathbf{W}_b$ or $\mathbf{W}_f$ is evaluated. Equations 3 and 4 assume that the spin system is in a single conformation characterized by the distances r_{ij}, and is undergoing isotropic rotational diffusion characterized by τ_c. The intensity of the $i \leftarrow j$ cross-peak in a two-dimensional TRNOESY experiment representing polarization transfer from j to i, for a mixing time τ_m, is given by (*15*)

$$m_{i\leftarrow j}(\tau_m) = (e^{-\mathbf{R}\tau_m})_{ij} M_{0j} = [\mathbf{I} - \mathbf{R}\tau_m + {}^1/_2\mathbf{R}^2\tau_m^{\,2} - {}^1/_6\mathbf{R}^3\tau_m^{\,3} + ...]_{ij} M_{0j} \quad (5)$$

where $\mathbf{I}$ is the $n \times n$ unit matrix. Equation 5 shows that, for short mixing times, the build-up of intensity of a cross-peak in a TRNOESY spectrum is a polynomial in τ_m, and the initial slope of the build-up curve is given by the linear term $\mathbf{R}_{ij}$. Since usually $\tau_c^{\,b} \sim 10$ ns, $\tau_c^{\,f} \sim 0.1$ ns, and $(\omega\tau_c^{\,b})^2 \gg 1$, if 10−25% of the ligand is bound, so that $p_b \approx 0.1-0.25$, eqs 2 and 4 lead to

$$\mathbf{R}_{ij} \approx p_b(\mathbf{W}_b)_{ij} \approx \frac{\gamma^4\hbar^2 p_b \tau_c^{\,b}}{10(r_{ij}^{\,b})^6} \quad (6)$$

Therefore, the ratios of the initial slopes for spin pairs are related to the corresponding internuclear distances in the bound conformation by

$$\frac{\mathbf{R}_{ij}}{\mathbf{R}_{kl}} \approx \left(\frac{r_{kl}^{\,b}}{r_{ij}^{\,b}}\right)^6 \quad (7)$$

The distance $r_{ij}^{\,b}$ can be estimated by using a calibration

distance if such a distance can be identified within the spin system. $p_b\tau_c^b$ may be evaluated from eq 6. It may be seen that the cross-peak intensities in a TRNOESY spectrum for a ligand in fast exchange between bound and free forms are similar to those of an intact system with an effective correlation time given by $p_b\tau_c^b$. Spin diffusion effects are contained in the quadratic and higher-order terms in eq 5 for a system of more than two spins.

Molecular Modeling. Molecular dynamics (MD) simulations and energy minimizations were carried out on a Silicon Graphics Octane computer, running Irix 6.4, using the program SYBYL6.5 from Tripos Inc., St. Louis, MO. Tripos force field was used for all the energy calculations, and the conjugate gradient algorithm was chosen for the minimization. The simulations and calculations were performed on ATP, AMP, and AMPPNP molecules (including the phosphate groups) in a vacuum.

RESULTS AND ANALYSIS

TRNOESY experiments were performed on AKe·Mg(II)-ATP, AKe·AMP·Mg(II)GDP, AKe·AMPPNP, and AKe·Mg-(II)AMPPNP complexes. Complexes with the ATP analogue, AMPPNP, were studied in order to make a comparison with the X-ray results, and measurements were made with and without Mg(II) for two reasons. First, in the X-ray data the cation was not located, and therefore, it is not known how the cation is chelated to the analogue. Second, since cation-chelated nucleotide binds only at the Mg(II)ATP site, the presence of the cation produces a selectivity for binding to this site. Sample conditions for the experiments were optimized such that nonspecific binding effects, and possible binding of the nucleotide of interest at the other site, are minimized. This was done by performing two sets of preliminary TRNOESY measurements described below.

Sample Protocol Determination. To minimize the NOE contribution from nonspecific binding, the sample protocols for the TRNOESY experiments were determined by following published procedures (*15*). TRNOESY experiments, each with a mixing time of 120 ms, were performed (at 500 MHz) on a set of AKe·Mg(II)ATP and AKe·AMP samples, in which the ligand concentration was varied from 2 to 12 mM while keeping the ligand-to-enzyme concentration ratio fixed at a value of 10:1. The dissociation constants for ATP and AMP binding to AKe were determined to be less than ∼80 μM. For AMP, binding at both sites has been suggested (see below), albeit about 3-fold weaker at the ATP site (*36*). These values suggest that even at the lowest concentrations chosen in these measurements, the primary sites of the respective nucleotides are occupied. The fractional NOEs observed in these experiments as a function of the ligand concentration for H1′−H2′—this interproton distance remains practically unchanged, 2.9 ± 0.2 Å, for all sugar puckers and glycosidic torsions—is shown in Figure 3. The fractional NOE for ATP increased by a factor of ∼3 when ligand concentration was changed from low (<5 mM) to high (∼10 mM) values, whereas the increase for AMP was relatively gradual and less than a factor of 2. Thus, nonspecific binding is greater for Mg(II)ATP than for AMP and is insignificant for ligand concentration ≤ ∼5.0 mM (with enzyme concentration ≤ ∼0.5 mM). Therefore, ∼ 0.5 mM enzyme concentration was used for all TRNOESY measurements, and nucleotide concentrations were chosen to be ∼4−6-fold larger than the enzyme concentration in order to maximize the fractional NOE by maximizing the active-site occupation of the nucleotides and at the same time to minimize the weaker nonspecific binding.

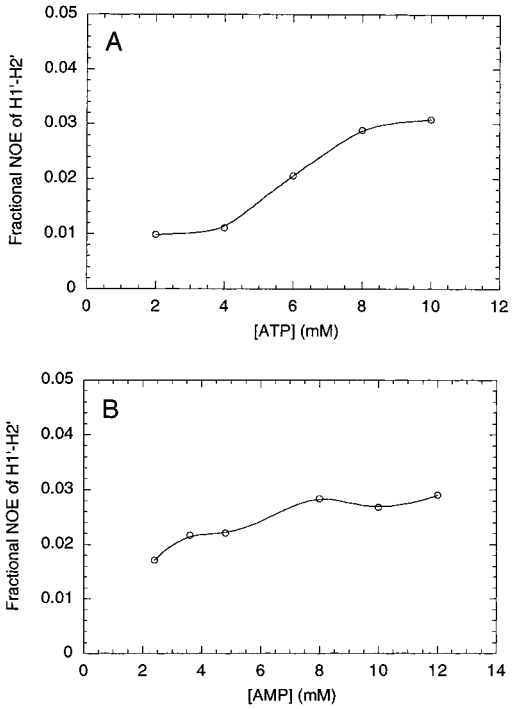

FIGURE 3: Dependence of fractional NOE (at 500 MHz) for the H1′−H2′ proton pair in AKe·Mg(II)·ATP (A) and AKe·AMP (B) complexes on ligand concentration. Nucleotide concentrations were varied from 1 to 12 mM, keeping the nucleotide-to-enzyme concentration ratio constant at 10:1. The samples were buffered in 50 mM Tris-d_{11}-HCl, pH 8.0, and measurements were made at 15 °C with a mixing time of 120 ms.

Mg(II)GDP Titration Experiment. As stated above, previous NMR and kinetic studies on adenylate kinase (*36*) suggested that AMP may bind to both sites, viz., the highly adenine-specific AMP site, which does not bind metal-bound nucleotides, and the Mg(II)ATP site, which binds ATP/ADP as well as GTP/GDP, with and without Mg(II). Therefore, while the TRNOESY data for Mg(II)ATP and Mg(II)-AMPPNP complexes are likely to arise from binding at the Mg(II)ATP site alone, it is possible that the NOEs observed in the AKe·AMP complex may be due to combined contributions from AMP bound to both sites. Since adenylate kinase also catalyzes the reaction AMP + Mg(II)GTP ⇔ ADP + Mg(II)GDP, Mg(II)GDP was used to block the possible binding of AMP to the Mg(II)ATP site without the reaction taking place. Fortunately, the NOE cross-peaks of Mg(II)GDP are readily distinguishable from those of AMP (see Figure 4B). Mg(II)GDP titration experiments were thus devised to determine an appropriate GDP concentration such that the NOEs of AMP would be exclusively from the AMP site. TRNOESY measurements were made, for a mixing time of 120 ms, on several samples of AKe·AMP·Mg(II)GDP in which the GDP concentration was varied while the enzyme and AMP concentrations were unchanged. The ratio of GDP and Mg(II) concentrations was kept 1:2 in all these experiments. It was found that the decrease of the H1′−H2′ NOE of AMP reached a plateau when the GDP concentration was 4-fold that of AMP, indicating a complete exclusion of AMP

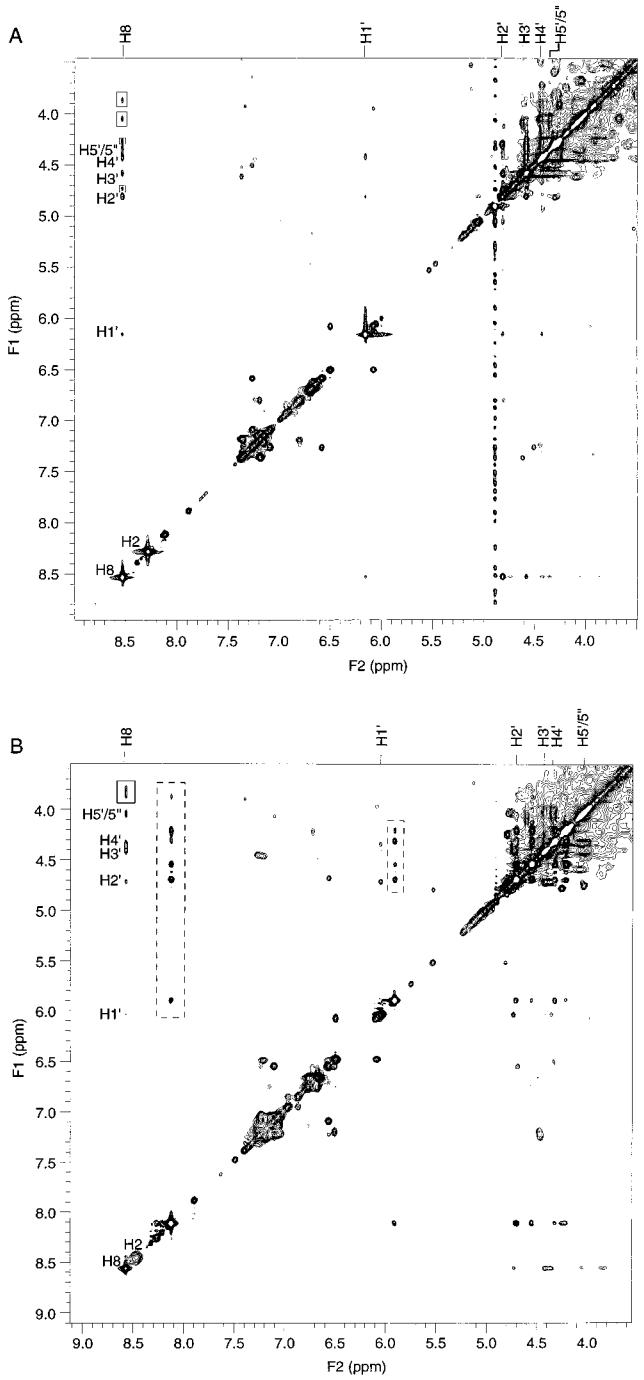

FIGURE 4: Proton TRNOESY spectra of AKe-bound ATP and AMP complexes. The samples were buffered in 50 mM Tris-d_{11}-HCl, pH 8.0, and measurements were made at 15 °C. Chemical shifts are referenced to DSS. (A) AKe·Mg(II)ATP, sample contained 0.49 mM AKe, 2.84 mM ATP, and 6.72 mM $MgCl_2$, and data were obtained at 720 MHz. (B) AKe·AMP·Mg(II)GDP; sample contained 0.48 mM AKe, 2.18 mM AMP, 4.30 mM GDP, and 8.20 mM $MgCl_2$, and data were obtained at 500 MHz. NMR parameters: 256 × $2t_1$ increments, 32 scans each; relaxation delay, 2 s; and mixing time, 120 ms. See text for other details. Intermolecular NOEs between the protein and nucleotide protons are marked by boxes of solid lines in both panels A and B. Cross-peaks arising from H8 and H1′ of GDP in panel B are marked by boxes of dotted lines.

binding to the Mg(II)ATP site. This ratio was maintained in subsequent experiments with AKe·AMP·Mg(II)GDP.

TRNOESY Spectra. Panels A and B of Figure 4 show the representative 2D TRNOESY spectra at a mixing time of 120 ms for the AKe·Mg(II)ATP and AKe·AMP·Mg(II)GDP complexes, respectively. For all nucleotides, H5′ and H5″ resonances coalesced to a single peak. The resonances were broadened enough so that spin−spin multiplicity was not resolved in any of the adenosine resonances. It may be noted that the spectra show some intermolecular NOEs between the protons of the protein and the ligand, in addition to the intramolecular NOEs between protons of the ligand.

Intramolecular NOE of Nucleotides in AKe-Bound Complexes. All the 2D TRNOESY spectra of AKe-bound complexes showed strong H8−H2′ and H8−H3′ NOE cross-peaks, indicating an anti conformation of the nucleotide. For all the nucleotides in their respective enzyme-bound complexes, strong NOEs include H8−H2′, H8−H3′, H1′−H2′, H1′−H4, H2′−H3′, H3′−H4′, H3′−H5′/5″, and H4′−H5′/5″, among which the last three overlap appreciably with neighboring cross-peaks from the protein. NOEs of H8−H1′ and H8−H5′/5″ (for some complexes), although relatively weak, are well separated. H1′−H5′/5″ NOE was not observed for any complex. The H2′−H5′/5″ cross-peak is usually weak and overlapping with protein signals. For distance calculations, only the well-resolved cross-peaks, which allow the NOEs to be accurately measured, were used. Figure 5 shows the experimental data and the second-order polynomial fit of the NOE build-up curves of the four adenine nucleotides in their respective AKe-bound complexes. The agreement between the polynomial fits and experimental data is fairly good considering that the error in NOE measurement is about 10%. Although the deviation appears larger for the stronger NOEs, the fractional deviation is nearly the same for all the build-up curves. The interproton distances were calculated using the coefficients of the linear term in the polynomial fit together with the calibration distance of H1′−H2′, viz., 2.9 ± 0.2 Å, in eq 7. These distances, listed in Table 1, were given as constraints in subsequent molecular modeling. In general, uncertainties in the distances determined from TRNOESY in this manner arise primarily from that in the calibration distance, i.e., ∼±0.2 Å. Those arising from ∼10% experimental error in the NOE measurements are expected to be absorbed in this range. Several NOE build-up curves, such as H1′−H3′ for AKe·AMP·Mg(II)GDP, H8−H4′ for AKe·AMPPNP, and H8−H1′ and H8−H5′/5″ for AKe·Mg(II)AMPPNP complexes, showed a lag phase at short mixing times, indicating a distance over 4 Å between them. A range of 4 Å < d < 6 Å was used as a distance constraint for these proton pairs.

Since H5′ and H5″ coalesce into a single resonance, the observed NOEs with H5′/5″, such as H8−H5′/5″, is a combined contributions from both H5′ and H5″. An average distance can be calculated by taking half of the NOE build-up rate. If spin i has distances of r_{i1} and r_{i2} from H5′ and H5″, respectively, this average distance, r_{iavg}, is related to r_{i1} and r_{i2} by

$$r_{iavg} = \left(\frac{r_{i1}^{-6} + r_{i2}^{-6}}{2}\right)^{-1/6} \quad (8)$$

r_{iavg} does not equal the distance from spin i to either H5′ or H5″ except for the special case of $r_{i1} = r_{i2}$. It is obvious that $r_{i1} < r_{iavg} < r_{i2}$ holds if $r_{i1} < r_{i2}$. Although r_{i1} and r_{i2} cannot be specified explicitly, when NOE is observed, their upper bounds are limited by the maximum distance giving

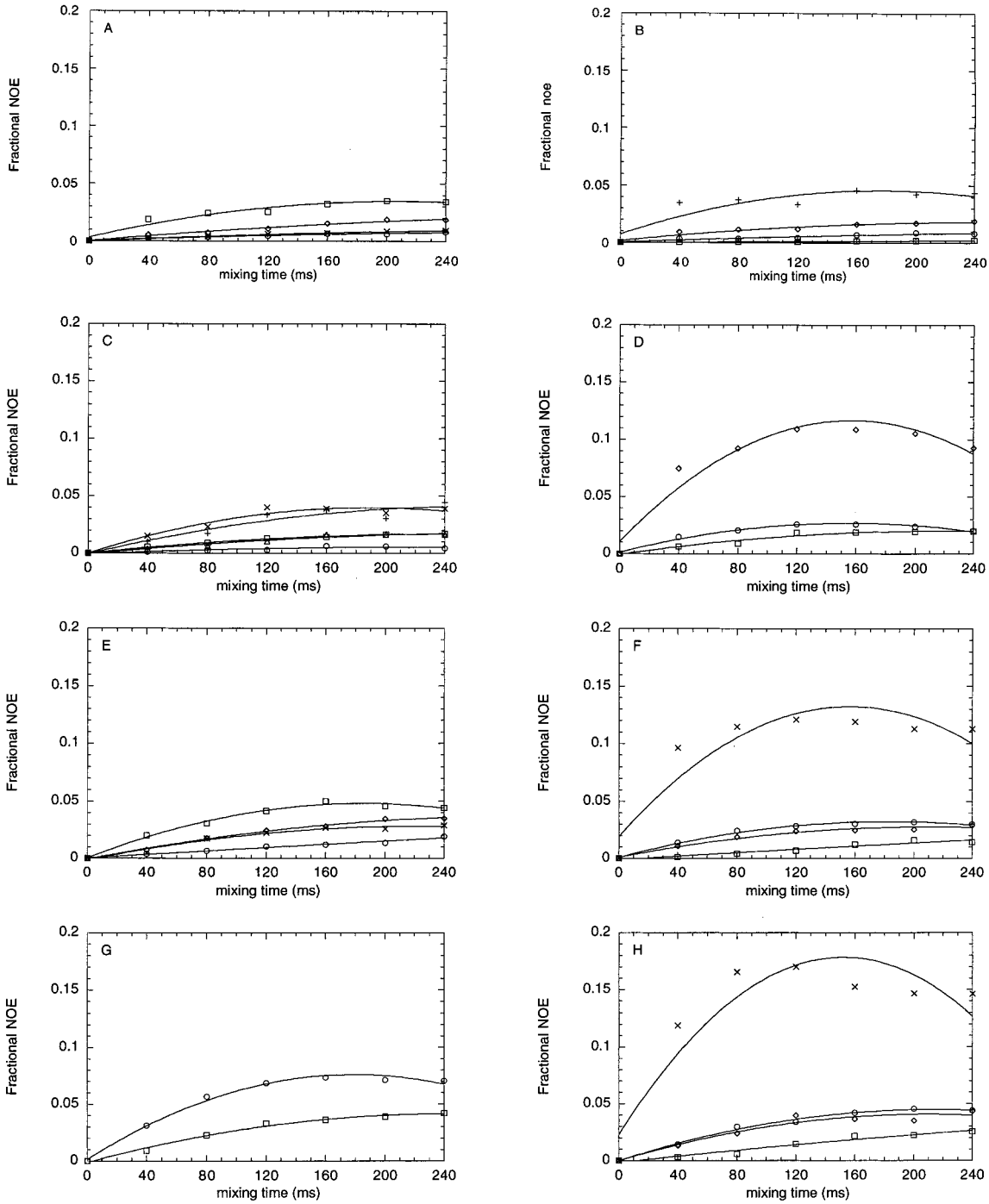

FIGURE 5: Fractional NOE build-up curves for adenine nucleotides in AKe-bound complexes. NOEs are for the following proton pairs: (A) H8−H1′ (○), H8−H2′ (□), H8−H3′ (◇), and H8−H5′/5″ (×) of AKe·Mg(II)ATP; (B) H1′−H2′ (○), H1′−H3′ (□), H1′−H4′ (◇), and H2′−H3′(+) of AKe·Mg(II)ATP; (C) H8−H1′ (○), H8−H2′ (□), H8−H3′ (×), H8−H4′ (+), and H8−H5′/5″ (△) of AKe·AMP·Mg(II)GDP; (D) H1′−H2′ (○), H1′−H4′ (□), and H2′−H3′(◇) of AKe·AMP·Mg(II)GDP; (E) H8−H1′ (○), H8−H2′ (□), H8−H3′ (◇), and H8−H5′/5″ (×) of AKe·AMPPNP; (F) H1′−H2′ (○), H1′−H3′ (□), H1′−H4′ (◇), and H2′−H3′(×) of AKe·AMPPNP; (G) H8−H2′ (○) and H8−H3′ (□) of AKe·Mg(II)AMPPNP; and (H) H1′−H2′ (○), H1′−H3′ (□), H1′−H4′ (◇), and H2′−H3′(×) of AKe·Mg(II)-AMPPNP. The solid lines are second-order polynomial fits of the experimental data. Sample conditions for ATP and AMP measurements are as given in the caption for Figure 3. For AMPPNP, the condition are the same except the following: AKe, 0.45 mM; AMPPNP, 2.75 mM; and $MgCl_2$, 5.7 mM [for AKe·Mg(II)AMPPNP complex], and data were obtained at 500 MHz.

observable NOEs, i.e., ∼5 Å, and their lower bounds by twice the van der Waals radius of a proton, ∼1.8 Å. Therefore, 1.8 Å< r_{i1} < r_{iavg} < r_{i2} < 5 Å was used as a general constraint, in which r_{i1} always represents the shorter of the two distances from spin *i* to H5′/H5″, in molecular modeling calculations.

Intermolecular NOEs. A few intermolecular NOEs between the protein and the ligand were observed in the 2D TRNOESY spectra. Since the spectra in the region of chemical shift < 4.90 ppm (the water signal) in both dimensions are crowded, intermolecular NOEs in this region were difficult to identify. However, the intermolecular NOEs for H8 and H1′ can be readily seen for all chemical shifts (no intermolecular NOEs were observed for H2). Some of these cross-peaks are shown in Figure 4, and a more complete set of chemical shifts is listed in Table 2. Table 2 shows

Table 1: Distance Constraints Determined from Analyses of TRNOESY Data of Adenine Nucleotides in Various Bound Complexes of AKe[a]

	AKe·Mg(II)ATP (Å)	AKe·AMP·Mg(II)GDP (Å)	AKe·AMPPNP (Å)	AKe·Mg(II)·AMPPNP (Å)
H8−H1′	4.0	3.9	3.7	4−6[b]
H8−H2′	2.2	3.4	2.7	2.6
H8−H3′	2.6	2.8	3.1	3.0
H8−H4′	n/a[c]	2.9	4−6[b]	3.3
H8−H5′/5″ [d]	2.9	3.4	3.0	4−6[b]
H1′−H2′	2.9	2.9	2.9	2.9
H1′−H3′	3.9	4−6[b]	3.7	3.5
H1′−H4′	2.5	3.2	3.1	2.9
H2′−H3′	2.0	2.3	2.3	2.3

[a] Errors in these distances are ±0.2 Å. [b] The NOE build-up curves for these proton pairs show a lag phase at short mixing times (see text). [c] H8−H4′ cross-peak of ATP overlaps with a protein NOE cross-peak that has significant relative intensity, especially for mixing times shorter than ∼120 ms. (Note that the protein and ligand NOEs have different dependence on mixing times.) [d] Distance (r_{iavg}) calculated from half the NOE build-up rate (see text).

Table 2: Chemical Shifts[a] of the Protein Protons Showing Intermolecular NOEs with the Nucleotide Protons H8 and H1′ in Various AKe-Bound Complexes

AKe·Mg(II)ATP (ppm)	AKe·AMP·Mg(II)GDP (ppm)	AKe·AMPPNP (ppm)	AKe·Mg(II)·AMPPNP (ppm)
Nucleotide Proton H8			
4.73			
4.26		4.22[b]	4.23
			4.18
4.05			
3.87	3.83[b]	3.80	3.80
1.03			
Nucleotide Proton H1′			
		2.04	2.04
		1.85[c]	1.89[c]
1.20	1.15	1.18	1.13
			1.02[c]
0.26	0.32	0.34	0.38

[a] Chemical shifts are referenced to DSS. [b] Location of resonance peaks complicated by spectral overlap. [c] Weak cross-peaks.

that the intermolecular NOE patterns of AKe·AMPPNP and AKe·Mg(II)AMPPNP complexes are similar to each other and to that of AKe·Mg(II)ATP. This pattern differs significantly from that of AKe·AMP·Mg(II)GDP. The specific amino acid residues from which these cross-peaks arise, have not been unequivocally identified, however.

Effect of Protein Protons on NOE-Determined Distances. As a few ligand−protein NOEs were observed in 2D TRNOESY spectra of the AKe−nucleotide complexes studied, it raises the question of reliability of the distances calculated from eq 7 without including the protein protons. This question is relevant irrespective of whether these cross-peaks are observed in the TRNOESY spectra or not, because they are not readily observed in complexes of heavy proteins due to line broadening, although magnetization transfer does occur between the protons of the ligand and the protein (*31*, *37*−*40*). The latter situation occurred in previously published TRNOESY studies of ATP-utilizing enzymes (*15*−*19*). However, a realistic estimate of the effect of such magnetization transfer could not be made in those cases due to lack of information on the protein structures.

The availability of the X-ray structure of AKe·AMP·AMPPNP (*5*) makes it possible to assess the effect of protein residues in the vicinity on the intramolecular NOEs of the nucleotide in the present work. This was accomplished by using the program CORCEMA, developed by Moseley et al. (*39*, *40*), which allows the calculation of TRNOE build-up curves for the ligand on the basis of input data consisting of the X-ray structure of a protein−ligand complex, by calculating the relaxation matrix, **R**, as given in eqs 2−5 for fast exchange (the program can be used even if the fast exchange condition is not valid). Protons of the ligand and protein can be included to the extent specified by the user. To provide the input data for the NOE calculations, hydrogens were added to both the enzyme and the nucleotides in the X-ray structure of AKe·AMP·AMPPNP (*5*), by using the program SYBYL. This was followed by energy minimization, in which all heavy atoms of the protein were defined as an aggregate so that only protons were allowed to relax during the energy minimization. The intramolecular NOEs of the ligands were calculated by including protein protons within shells of various sizes surrounding the ligand. For example, a shell of 3 Å was defined to include all the residues that have at least one proton located within 3 Å of any nonexchangeable proton of the ligand. Such NOE calculations were made for shells of 3, 5, and 10 Å, which contain 8, 18, and 54 residues, respectively. Other input data for CORCEMA include a proton frequency of 720 MHz, isotropic correlation times of 0.1 ns for free ligands and 20 ns for the enzyme and enzyme-bound complexes, enzyme concentration of 0.5 mM, nucleotide concentration of 2.5 mM, and a dissociation constant of 0.1 mM for both AMP and AMPPNP. In addition, leakage rates representing spin−lattice relaxation due to mechanisms other than intramolecular proton dipole−dipole interaction have been added to the diagonal elements of the relaxation matrix. The rates were 1.0 s^{-1} and 2.0 s^{-1} for the free and bound species, respectively. The simulations were made for mixing times of 40, 80, 120, 160, 200, and 240 ms, similar to those used in the experiments.

Before discussing the results of the simulations, it should be noted that the nucleotide conformation in these calculations is that given by the X-ray structure, whereas the goal is to evaluate the effect of protein protons on the TRNOESY-determined nucleotide conformation, which turns out to be different from the X-ray conformation (see below). However, the location of the protein protons with respect to the NMR-determined conformation is not known, and a simulation of this kind cannot be made. Therefore, to make a *realistic* estimate of the effect of protein protons, the X-ray structure of the enzyme−substrate complex, in which the coordinates of all the protons can be assigned, is chosen. Thus, while the errors estimated for specific interproton distances may not be precisely valid for the NMR conformation of the nucleotide, the ranges of these errors are likely to be similar because the two structures primarily differ in the glycosidic torsion angle and are qualitatively alike with reference to the general proximity of the protein and ligand protons.

The simulated build-up curves showed sizable differences for some proton pairs in the fractional NOEs calculated with and without including protein protons. In most cases the NOE decreases due to the inclusion of protein protons, and in a few cases it increases. Examples are shown in Figure 6,

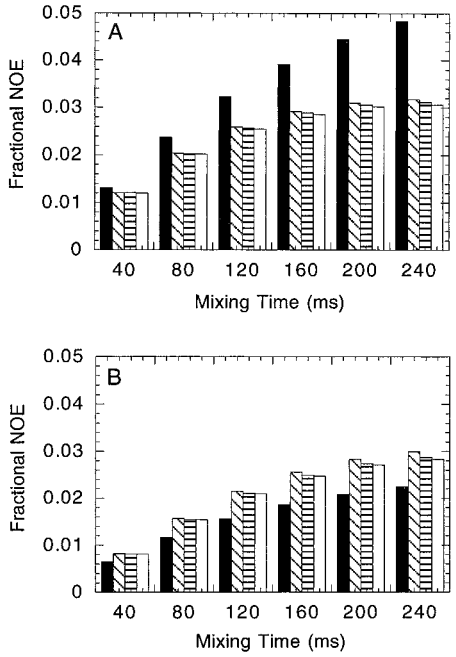

FIGURE 6: Fractional NOE of H1′−H2′ (A) and H1′−H4′ (B) of AMP calculated for various mixing times and shell sizes on the basis of X-ray structure of AKe·AMP·AMPPNP (*5*) using CORCEMA (*39*, *40*). For each mixing time, the four columns from left to right are NOEs calculated by including (i) no protein protons, and protein protons within shells of (ii) 3 Å, (iii) 5 Å, and (iv) 10 Å. Other input parameters used in the calculations are as follows: proton frequency, 720 MHz; correlation times, 0.1 and 20 ns for the free and bound species, respectively; leakage rates, 1.0 s^{-1} and 2.0 s^{-1}, respectively; enzyme concentration, 0.5 mM; nucleotide concentration, 2.5 mM; dissociation constant for the nucleotide, 0.1 mM.

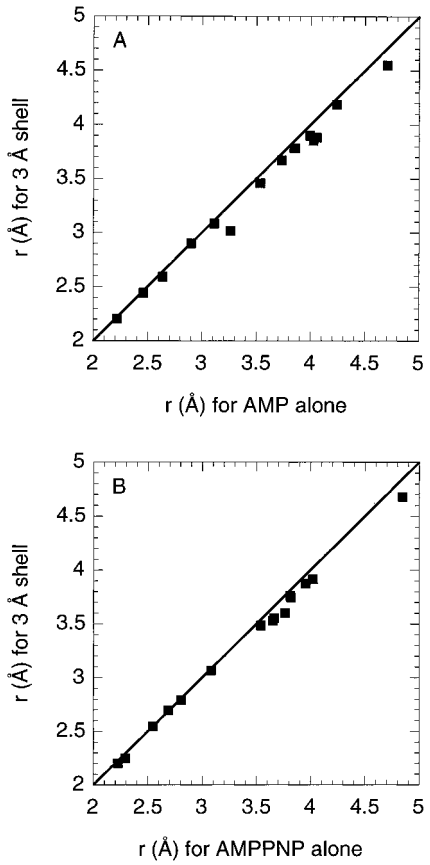

FIGURE 7: Comparison of distances calculated from the initial slopes of simulated NOEs by ignoring protein protons and including those located within a 3 Å shell for AMP (A) and AMPPNP (B), respectively. The calculations were performed on the basis of the X-ray structure of AKe·AMP·AMPPNP by using the program CORCEMA (see text). The solid line is drawn through the origin with a slope of unity.

panels A and B, in which the fractional NOEs of H1′−H2′ and H1′−H4′ of AMP, respectively, are plotted as a function of mixing time for different size of shells. It is evident that the effect of protein protons occurs primarily due to those in the 3 Å shell, as increasing the shell size further makes a negligible difference. By fitting the simulated build-up curves to a second-order polynomial, initial slopes of these curves were evaluated analogous to the procedure used in the analysis of the experimental data. The initial slopes with AMP protons alone are ∼14% larger for H1′−H2′, and ∼29% smaller for H1′−H4′ than those with protein protons within a 3 Å shell included. This deviation for H1′−H4′ is the largest among all proton pairs for both AMP and AMPPNP. The influence of the geometrical location of a spectator spin with respect to an interacting spin pair on the NOEs observed, and the distances derived from them, were theoretically calculated for a three-spin system (*41*). This theory provides a general explanation for the effect of protein protons seen in these calculations. The X-ray structure shows that one of the Hδ atoms of Arg 36 is located near H1′ and H4′ of AMP, with distances of 2.2 Å from H4′ and 2.7 Å from H1′. This geometrical arrangement basically accounts for the significant increase in the NOE seen for the H1′−H4′ pair. For other proton pairs, no protein protons were found interpolating in a similar manner.

From the initial slopes of the simulated TRNOESY build-up curves, evaluated as explained above, interproton distances were back-calculated on the basis of eq 7 by using the H1′−H2′ distance (2.9 ± 0.2 Å) as calibration. The calculated distances with and without including the proton proteins in the simulation differed by ∼8% for H1′−H4′ and <5% for all other proton pairs. Figure 7 panels A and B, respectively, show plots of interproton distances calculated for AMP and AMPPNP by including protein protons within a 3 Å shell against those with the nucleotide protons alone. It is seen that the agreement between the two sets of distances is generally good, and deviations begin to occur as the distance between proton pairs increases, as expected. Although inclusion of the protein protons may appreciably alter the NOE, the calculated interproton distances are not much affected for two reasons: (i) in most cases the NOE increases both for the proton pair of interest and for the calibration pair (H1′−H2′) so that the initial slope ratio in eq 7 is not significantly changed; and (ii) the distances are given by the sixth root of the initial slope ratio so that the effect of the deviations in NOE are scaled down, yielding errors no more than ∼8% in the distances calculated. Thus, the CORCEMA simulations indicate that protein-mediated spin diffusion is not a significant factor in the reliability of interproton *distances* calculated by analyzing the TRNOESY data as presented here.

Molecular Modeling of Adenosine Conformation. Adenosine conformations compatible with the NOE-determined distances for the adenine nucleotides in AKe-bound complexes were obtained by using the software package SYBYL. A typical protocol of the structure calculation was the

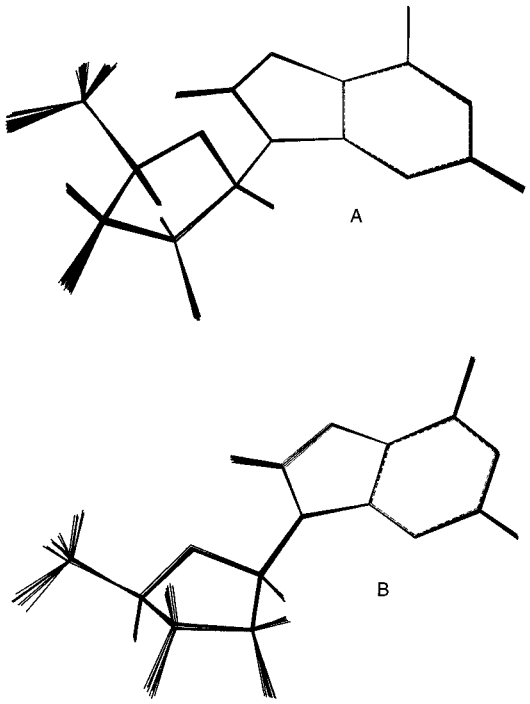

FIGURE 8: Pictorial representation of adenosine conformations of ATP and AMP bound at the active sites of AKe in AKe·Mg(II)-ATP (A) and AKe·AMP·Mg(II)GDP (B) complexes, respectively.

following. A total of 40 free nucleotide molecules (without distance constraints) were generated by MD simulated annealing, in which the nucleotide structure is repeatedly heated to 2000 K and allowed to equilibrate at this temperature for 2 ps, followed by exponential cooling to 300 K over 5 ps. Energy minimization was then performed on these nucleotide structures with the NOE-derived distances given as constraints (Table 1). For those distances not involving H5′/5″, a constraint range of ±5% of each value was allowed, and for those involving H5′/5″, a general constraint, 1.8 Å < r_{i1} < r_{iavg} < r_{i2} < 5 Å, was used as explained earlier. A force constant of 200 kcal/(mol·Å) was chosen for all the constraints and in all the energy minimizations. An ensemble of adenosine conformations for both ATP and AMP, deduced from these computations, are shown in Figure 8, panels A and B, respectively. The RMSD of the fit upon matching the heavy atoms of adenosine is found to be <0.13 Å for all the ensembles. The mean values of interproton distances and the various torsion angles in such converged structural ensembles are given in Tables 3 and 4. For AKe·Mg(II)-ATP, AKe·AMP·Mg(II)GDP, AKe·AMPPNP, and AKe·Mg(II)AMPPNP complexes, the glycosidic torsion angle, χ, are 51° ± 5°, 37° ± 5°, 49° ± 5°, and 47° ± 5°, and the pseudorotational phase angles, P, of the sugar puckers are 70° ± 5°, 50° ± 5°, 79° ± 5°, and 103° ± 5°, respectively. Also included in Tables 3 and 4 are the values of the corresponding interproton distances and various torsion angles measured from the X-ray structures. It is evident that the adenosine conformations deduced from NMR and X-ray methods are significantly different.

DISCUSSION

In the present TRNOESY study, no intermolecular NOE between the nucleotide and the protein resonances in the

Table 3: Mean Values of Interproton Distances[a] with Adenosine Moieties in the Calculated Structural Ensembles for Different AKe-Bound Nucleotide Complexes

	complexes					
	NMR				X-ray AKe·AMP·AMPPNP	
proton pairs	AKe·Mg(II)ATP	AKe·Mg(II)AMPPNP	AKe·AMPPNP	AKe·AMP·Mg(II)GDP	AMP	AMPPNP
H8−H2	6.4	6.5	6.5	6.5	6.4	6.5
H8−H1′	3.2	3.9	3.8	3.9	3.5	3.9
H8−H2′	2.2	2.6	2.7	3.3	4.3	2.2
H8−H3′	2.6	2.9	3.1	2.9	3.8	4.3
H8−H4′	3.9	4.1	4.5	4.6	4.8	5.0
H8−H5′	4.1	4.3	4.2	4.4	4.8	4.6
H8−H5″	2.7	4.0	2.8	3.2	4.3	3.8
H2−H1′	5.0	5.0	4.8	4.7	5.2	4.7
H2−H2′	6.4	6.2	6.2	5.8	4.0	7.0
H2−H3′	8.1	7.9	8.0	7.8	6.2	8.6
H2−H4′	7.6	7.7	7.7	7.7	7.5	7.6
H2−H5′	8.8	9.6	8.8	9.0	8.9	8.8
H2−H5″	8.5	9.0	8.5	8.8	8.7	7.3
H1′−H2′	3.0	2.9	2.9	2.9	2.9	3.0
H1′−H3′	3.8	3.7	3.8	4.0	4.0	4.0
H1′−H4′	2.6	3.0	3.0	3.0	3.2	3.6
H1′−H5′	4.3	5.0	4.6	4.6	5.1	5.1
H1′−H5″	4.2	4.8	4.5	4.7	4.5	4.3
H2′−H3′	2.1	2.1	2.3	2.4	2.4	2.5
H2′−H4′	3.8	4.0	4.1	3.8	3.7	3.9
H2′−H5′	5.0	4.7	5.1	5.4	4.8	4.1
H2′−H5″	3.9	5.1	4.0	4.6	5.1	4.0
H3′−H4′	3.1	2.9	3.0	3.1	3.1	2.6
H3′−H5′	3.7	2.7	3.6	3.7	2.7	2.9
H3′−H5″	2.4	3.6	2.4	2.6	3.6	3.8
H4′−H5′	2.9	2.5	2.5	2.5	2.7	2.3
H4′−H5″	3.1	2.4	3.1	3.1	2.3	2.6
H5′−H5″	1.8	1.8	1.8	1.8	1.8	1.8

[a] These distances are given in angstroms and vary over an approximate range of ±5−10% of their values. The corresponding distances in the X-ray data (*5*) are shown for comparison.

Table 4: Mean Values of Various Torsion Angles and the Pseudorotation Parameters of the Sugar Ring in the Calculated Structural Ensembles for AKe-Bound Nucleotides[a]

torsions[b] and pseudorotation parameters[c]	complexes					
	NMR				X-ray AKe·AMP·AMPPNP	
	AKe·Mg(II)ATP	AKe·Mg(II)AMPPNP	AKe·AMPPNP	AKe·AMP·Mg(II)GDP	AMP	AMPPNP
χ	51	47	49	37	−4	83
γ	−56	65	−56	−61	74	37
ν_0	−28	−28	−26	−21	−9	4
ν_1	9	20	12	−5	−19	14
ν_2	12	−6	6	26	38	−26
ν_3	−28	−10	−21	−39	−42	26
ν_4	35	23	29	39	35	−20
P	70	103	79	50	30	204
α	34	27	29	40	44	29

[a] These values are given in degrees and span an approximate range of ±5°. The corresponding parameters in the X-ray data (*5*) are shown for comparison. [b] These torsions are denoted as follows: χ (O4′−C1′−N9−C8), γ (O5′−C5′−C4′−C3′), ν_0 (C4′−O4′−C1′−C2′), ν_1 (O4′−C1′−C2′−C3′), ν_2 (C1′−C2′−C3′−C4′), ν_3 (C2′−C3′−C4′−O4′), and ν_4 (C3′−C4′−O4′−C1′). For example, χ is 0° when the O4′−C1′ and N9−C8 are eclipsed and a counterclockwise rotation about the C1′−N9 bond is defined as a positive angle. [c] $P = \tan^{-1}[(\nu_4 + \nu_1) - (\nu_3 + \nu_0)/2\nu_2(\sin 36° + \sin 72°)]$; and $\alpha = \nu_2/\cos P$ are the phase angle and the amplitude of pseudorotation of the sugar ring, respectively. When ν_2 is negative, 180° is added to the calculated value of P.

aromatic region has been observed. This agrees with the results of Vetter et al. (*10*) for AKe·AMP, AKe·ATP, and AKe·Mg(II)ATP complexes. However, it may be noted parenthetically that these authors reported NOEs of H2 of the putative Mg(II)ATP fragment of Mg(II) AP_5A with two protein aromatic resonances in the ternary complex AKe·Mg(II)AP_5A. Although the protein resonances listed in Table 2 cannot be positively identified, those with chemical shifts between 3.8 and 5.0 ppm are most likely to be from α-protons. A comparison with the X-ray structures of both AKe·AP_5A (*4*) and AKe·AMP·AMPPNP (*5*) suggests that the signal at 3.83 ppm for the AKe·AMP·Mg(II)GDP complex is likely to be from Gly 85. The intermolecular NOEs observed in the TRNOESY spectra between protein and nucleotide protons are nearly identical (Table 2) for AKe·AMPPNP and AKe·Mg(II)AMPPNP, indicating that the microenvironment of AMPPNP in AKe is essentially the same with and without Mg(II) and is similar to that seen with Mg(II)ATP. The adenosine conformations derived for the two complexes are also very similar, suggesting that AMPPNP binds only at the Mg(II)ATP site, even without the presence of Mg(II).

The NOE calculations on the basis of the proton locations compatible with the published X-ray structure of AKe·AMP·AMPPNP were useful for a realistic qualitative evaluation of the role of the magnetization transfer between protein and ligand protons on the TRNOESY data and on the interproton distances determined for the bound ligand (*31, 37−40*). The calculations showed that discrepancies between NOEs arise primarily from protein protons in the immediate vicinity, <3 Å, of the ligand and that errors with distances determined are usually <±5%, except in one case where it is ∼8%. It should be noted, however, that adenylate kinase is a light protein of molecular mass ∼24 kDa, and a rotational correlation time of ∼20 ns was used in the computation. The rate of polarization transfer to the protein protons will be larger for larger proteins with longer correlation times. Furthermore, the effect of protein protons on the ligand NOEs depends on the geometrical location of the spectator protons on the protein with respect to the ligand proton pairs (*41*). Thus, although the participation of the protein protons does not cause significant errors in the structures deduced here, the effect is not evanescent and should be considered in evaluating the precision of the structures derived from TRNOESY data and the interpretations made thereof.

The conformations obtained for Mg(II)ATP, AMPPNP, and Mg(II)AMPPNP, which all bind at the Mg(II)ATP site, have glycosidic torsion angles within 48° ± 3°, in good agreement with the range of 52° ± 8°, previously measured for other ATP-utilizing enzymes (*15−19*). The glycosidic angle of AMP in the AKe·AMP·Mg(II)GDP complex is 37°, which lies somewhat outside this range, although not dramatically different. There is a seemingly appreciable variability in the sugar puckers deduced for the nucleotide structures as indicated, for example, by the values of P in Table 4. However, it should be noted that the sugar pucker is not particularly sensitive to most of the interproton distances in the ribose other than H3′−H4′ and H1′−H4′ (*42*). Therefore, the variation in P may not be significant. The adenosine conformations determined for various complexes differ significantly from those in the X-ray structures of AKe-bound complexes. The differences suggest that, during the crystallization process, the nucleotides may have been trapped in unproductive conformations.

The adenosine conformations of ATP and AMP bound at the active site of AKe have been deduced in the present study. The location of the cation with respect to the phosphates, and the orientation of the phosphate chain with respect to the adenosine moieties of ATP and AMP are determined by means of relaxation measurements in the presence of activating paramagnetic cations [Co(II) and Mn(II)]. The availability of additional distance constraints from such measurements help to refine the adenosine conformations deduced here. All the structural data taken together allow a complete characterization of the conformations of both substrates of AKe. These results are presented in the accompanying paper (*22*).

ACKNOWLEDGMENT

We are grateful to Professor Paul Rösch, Universität of Bayreuth, Bayreuth, Germany, and his research group for providing us with the expression system and associated procedures for preparing the protein, to Professor N. R.

Krishna, University of Alabama, Birmingham, AL, for the CORCEMA program, to Dr. Nagarajan Murali, National High Magnetic Field Laboratory (NHMFL), Tallahassee, FL, for help and advice with experiments at 720 MHz performed there, and to Dr. Daniel H. Robertson at the Facility for Computational Molecular Science, IUPUI, for helpful suggestions. Thanks are due to Drs. Bruce Ray, Steve Landy, Gotam Jarori, Vidya Raghunathan, Mei H. Chau, and Ms. Marina Lyshevski of the NMR group at IUPUI for assistance received in various ways during this research.

SUPPORTING INFORMATION AVAILABLE

A table showing the glycosidic torsion angles, χ, measured for the enzyme-bound adenine nucleotides from the X-ray structures available in the Brookhaven Protein Data Bank up to May 1999. The kinases included in this database all have a small molecule for the second substrate. Protein kinases are not included. This material is available free of charge via the Internet at http://pubs.acs.org.

REFERENCES

1. Colowick, S. P., and Kalckar, H. M. (1943) *J. Biol. Chem. 148*, 117.
2. Noda, L. (1973) in *The Enzymes 8*, pp 279−305, Academic Press, New York.
3. Müller, C. W., Schlauderer, G. J., Reinstein, J., and Schulz, G. E. (1996) *Structure 4*, 147−156.
4. Müller, C. W., and Schulz, G. E. (1992) *J. Mol. Biol. 224*, 159−177.
5. Berry, M. B., Meador, B., Bilderback, T., Liang, P., Glaser, M., and Philips, G. N., Jr. (1994) *Proteins: Struct., Funct., Genet. 19*, 183−198.
6. Tsai, M. D., and Yan, H. (1991) *Biochemistry 30*, 6806−6818, and references cited therein.
7. Egner, U., Tomasselli, A. G., and Schulz, G. E. (1987) *J. Mol. Biol. 195*, 649−658.
8. Müller, C. W., and Schulz, G. E. (1988) *J. Mol. Biol. 202*, 909−912.
9. Schulz, G. E., Müller, C. W., and Diederichs, K. (1990) *J. Mol. Biol. 213*, 627−630.
10. Vetter, I. R., Reinstein, J., and Rösch, P. (1990) *Biochemistry 29*, 7459−7467.
11. Vetter, I. R., Konrad, M., and Rösch, P. (1991) *Biochemistry 30*, 4137−4142.
12. Yan, H., and Tsai, M.-D. (1991) *Biochemistry 30*, 5539−5546.
13. Schlarder, G. J., and Schulz, G. E. (1996) *J. Mol. Biol. 256*, 223−227.
14. Abele, U., and Schulz, G. E. (1995) *Protein. Sci. 4*, 1262−1271.
15. Murali, N., Jarori, G. K., Landy, S. B., and Nageswara Rao, B. D. (1993) *Biochemistry 32*, 12941−12948.
16. Murali, N., Jarori, G. K., and Nageswara Rao, B. D. (1994) *Biochemistry 33*, 14227−14236.
17. Jarori, G. K., Murali, N., and Nageswara Rao, B. D. (1994) *Biochemistry 33*, 6784−6791.
18. Murali, N., Lin, Y., Mechulam, Y., Plateau, P., and Nageswara Rao, B. D. (1997) *Biophys. J. 70*, 2275−2284.
19. Jarori, G. K., Murali, N., Switzer, R. L., and Nageswara Rao, B. D. (1995) *Eur. J. Biochem. 230*, 517−524.
20. Zhou, G., Somasundaram, T., Blanc, E., Parthasarathy, G., Ellington, W. R., and Chapman, M. S. (1998) *Proc. Natl. Acad. Sci. U.S.A. 95*, 8449−8454.
21. Nageswara Rao, B. D., and Ray, B. D. (1992) *J. Am. Chem. Soc. 114*, 1566−1573.
22. Lin, Y., and Nageswara Rao, B. D. (2000) *Biochemistry 39*, 3647−3655.
23. Reinstein, J., Brune, M., and Wittinghofer, A. (1988) *Biochemistry 27*, 4712−4720.
24. Brune, M., Schumann, R., and Wittinghofer, A. (1985) *Nucleic Acids Res. 13*, 7139−7151.
25. States, D. J., Haberkorn, R. A., and Ruben, D. J. (1982) *J. Magn. Reson. 48*, 286−292.
26. Macura, S., Huang, Y., Sueter, D., and Ernst, R. R. (1981) *J. Magn. Reson. 43*, 259−281.
27. Campbell, A. P., and Sykes, B. D. (1991) *J. Magn. Reson. 93*, 77−92.
28. Ni, F. (1992) *J. Magn. Reson. 96*, 651−656.
29. Lee, W., and Krishna, N. R. (1992) *J. Magn. Reson. 98*, 36−48
30. London, R. E., Perlman, M. E., and Davis, D. G. (1992) *J. Magn. Reson. 97*, 79−98.
31. Zheng, J., and Post, C. B. (1993) *J. Magn. Reson. B101*, 262−270.
32. Landy, S. B., and Nageswara Rao, B. D. (1989) *J. Magn. Reson. 81*, 371−377.
33. Abragam, A. (1961) *Principles of Nuclear Magnetism*, Oxford University Press, London.
34. Noggle, J. H., and Schirmer, R. E. (1971) *The Nuclear Overhauser Effect*, Academic Press, New York.
35. Keepers, J. W., and James, T. L. (1984) *J. Magn. Reson. 57*, 404−426.
36. Reinstein, J., Vetter, I. R., Schlichting, I., Rösch. P., Wittinghofer, A., and Goody, R. S. (1990) *Biochemistry 29*, 7440−7450.
37. Ni, F., and Zhu, Y. (1994) *J. Magn. Reson. B102*, 180−184.
38. Jackson, P. L., Mosley, H. N. B., and Krishna, N. R. (1995) *J. Magn. Reson. B107*, 289−292.
39. Moseley, H. N. B., Curto, E. V., and Krishna, N. R. (1995) *J. Magn. Reson. B108*, 243−261.
40. Krishna, N. R., and Moseley, H. N. B. (1998) *Biol. Magn. Reson. 17*, 223−307.
41. Landy, S. B., and Nageswara Rao, B. D. (1989) *J. Magn. Reson. 83*, 29−43.
42. Hosur, R. V., Govil, G., and Miles, H. T. (1988) *Magn. Reson. Chem. 26*, 927−944.

BI991921T